Statistics of the transient frequency modulation in the switch-on of a single-mode semiconductor laser

Salvador Balle,* F. de Pasquale,† N. B. Abraham,‡ and M. San Miguel
Departament de Física, Universitat de les Illes Balears, E-07071 Palma de Mallorca, Spain
(Received 21 March 1991)

The variations of the optical frequency during the switch-on of a single-mode semiconductor laser diode have been studied. Our model relies on stochastic rate equations, and therefore a meaningful description of the laser frequency in the presence of both noise and transient evolution is difficult. The relation between an approximately instantaneous frequency that we calculate numerically and experimentally measured frequencies is discussed. We analyze the frequency variations during switch-on processes and the statistical properties of the nearly instantaneous frequency that we chose as the most reasonable to calculate. The range of the frequency chirp during the first pulse of the intensity is stochastic, but it is correlated with the switch-on time, and therefore its statistical properties can be deduced from those of the first-passage-time distribution. The correlations permit a single discriminator to select a subset of pulses with similar peak intensities, delay times, and chirp ranges. In addition, there are significant differences between the averaged quantities and results for a single switch-on.

PACS number(s): 42.55.Px, 42.50.Md, 42.50.Ar, 05.40.+j

I. INTRODUCTION

Statistical properties of the transient evolution of the output of a laser after it is switched on have been considered in a variety of situations for the past 20 years [1]. These transients involve both dynamical evolution and stochastic aspects with noise contributing the initial conditions as well as fluctuations during the dynamical evolution. The transients usually have been characterized either by ensemble averages of the intensity fluctuations [2, 3] or by the statistics of the switch-on time (passage-time statistics) [2, 4, 5]. These two characterizations refer to the evolution of the intensity.

A natural question is how to extend these studies to characterize the transient stochastic dynamics of the frequency and phase of the field. Recent experimental work [6] that shows the possibility of direct frequency and phase measurements makes this question experimentally meaningful. The coupling and interplay of phase and intensity fluctuations is expected to cause interesting effects. A first study [7] along this line has considered the effect of transient intensity fluctuations on phase fluctuations after the Q switching of a detuned class-A laser [8] (He-Ne, dye, etc.). However, the interplay of intensity and phase fluctuations is more relevant for semiconductor lasers due to the linewidth enhancement factor [9] α. The α factor determines the degree of coupling between the phase and intensity of the electric field, yielding nontrivial phase and frequency dynamics. The relatively large value of α for a single-mode semiconductor laser (SSL) means that the frequency variations during the transient reflect the evolution of the intensity [10]. And, because spectral variations within the duration of a pulse can contribute to pulse compression or signal distortion, there has been interest in this phenomenon in semiconductor lasers. There have been some studies of time-resolved spectra and spectral-resolved time evolution, but the experimental measurements have been of averages rather than single pulses [11–13].

Transient statistics for semiconductor lasers have been recently studied through consideration of the distribution of switch-on times [5, 14, 15], intensity fluctuations in the nonlinear regime [15, 16], and statistics of the maximum intensity in the first peak of the relaxation oscillations [15]. However, we are not aware of any study of the transient statistics of the frequency of semiconductor lasers.

An interesting feature of a SSL is the high sensitivity of the laser frequency to changes in the operating point of the system [10]. In particular, changes in the laser output intensity cause changes in the lasing frequency through associated changes in the number of carriers in the medium. This phenomenon, known as frequency modulation in general, leads to a nearly monotonic sweep (chirp) of the frequency during the first intensity pulse when a SSL is switched on. This frequency chirp has attracted both experimental and theoretical attention since it has obvious importance in dispersive degradation of signals in optical communications and in offering the possibility of pulse compression [17]. Most applications involve intensity modulation between a high-intensity state and a low-intensity one. In this case, both the intensity dynamics and the associated frequency variations have been satisfactorily analyzed from a deterministic point of view [18, 19].

However, the problem is far more sensitive to noise when the initial state is below the threshold for laser action [12]. It has been shown [14] that the fluctuations in both the switch-on time and the intensity are larger when the initial state is below threshold. In addition, analyses of steady-state power spectra [20, 21] find large linewidths for lasers below threshold. These results indicate the importance of spontaneous emission noise as

the laser is switched on from the off state. At later times, the evolution of the system is characterized by relaxation oscillations of the intensity and carrier number. During the oscillations the laser output can greatly exceed its steady-state value, emerging in the form of short pulses of high intensity [22]. As a consequence, the associated frequency chirping during each pulse can be very large and, more importantly, due to the intrinsic randomness of the laser switch-on process it turns out that the chirp varies from pulse to pulse.

The relatively large fluctuations in the amplitude and phase caused by spontaneous emission noise before the intensity reaches a macroscopic value clearly indicate that a deterministic analysis of the system evolution is not valid. Instead, we have to consider stochastic evolution equations based on the Langevin formulation of the rate equations for a SSL. Choosing units such that the laser intensity I (the carrier number N) corresponds to the number of photons (carriers) inside the active layer and taking a rotating reference frame such that the phase φ of the slowly varying amplitude of the electric field is constant in the nontrivial steady-state solution except for phase diffusion, these equations read [23]

$$\dot{I} = (G-\gamma)I + 4\beta N + \sqrt{4\beta N I}\xi_I(t) , \tag{1}$$

$$\dot{\varphi} = \frac{\alpha}{2}(G-\gamma) + \sqrt{(\beta N/I)}\xi_\varphi(t) , \tag{2}$$

$$\dot{N} = C - \gamma_e N - GI - \sqrt{4\beta N I}\xi_I(t) + \sqrt{\gamma_e N}\xi_N(t) , \tag{3}$$

$$G = \frac{g(N-N_0)}{\sqrt{1+sI}} . \tag{4}$$

The meanings and values of the different parameters involved in these equations are listed in Table I. These equations are derived from the semiclassical equations for the laser after performing an adiabatic elimination of the polarization. The gain G includes a saturation term of the form $(1+sI)^{-1/2}$, which has been recently proposed by Agrawal [24].

Spontaneous emission is taken into account by the term $4\beta N$ which yields the mean power emitted in the lasing mode, an intensity noise term $\sqrt{4\beta N I}\ \xi_I(t)$ which describes the fluctuations of this mean power, and a phase noise term $\sqrt{\beta N/I}\ \xi_\varphi(t)$ which describes the phase fluctuations in the electric field associated with the spontaneous emission. Obviously, phase fluctuations due to noise fluctuations are huge when the intensity is small.

Random nonradiative carrier decay is included by means of the noise term $\sqrt{\gamma_e N}\ \xi_N(t)$. However, the evolution of the carrier number during the transient is dominated by the mean value of the injection current C and the noise terms are important only around steady state [14–16].

The different noise sources are taken to be Gausssian of zero mean and correlations given by

$$\langle \xi_i(t)\xi_j(t')\rangle = 2\delta_{ij}\delta(t-t')\ i,j = I,\varphi,N . \tag{5}$$

The intensity and phase noise strengths used here are equivalent to a spontaneous emission strength $\sqrt{\beta N}$ for the complex electric field. This form of the spontaneous emission strength is a good approximation to the exact form that has been deduced from first principles for a system where the matter and the radiation have reached equilibrium [25]. When the matter-radiation equilibrium has not yet been achieved, the exact form of the spontaneous emission strength is unknown. Hence, assuming the validity of this spontaneous emission strength for systems in the transient regime cannot be justified in a rigorous way. Nevertheless, it has been previously used for studying the transient regime of semiconductor lasers and the results show reasonable evolution of the intensity and carrier number [14–16, 26].

The paper is organized as follows. In Sec. II we discuss how to describe the instantaneous frequency of the electric field in the presence of both noise and transient evolution. In Sec. III we analyze individual transients, from which we find that the chirp range along each trajectory is a stochastic quantity, and we show that the laser frequency is properly described by our approximation. In Sec. IV we study the statistical properties of the laser frequency modulation along the transient, paying special attention to the frequency chirp during the first intensity pulse. We find that the statistical properties of the laser frequency are correctly described in our approximation. Finally, in Sec. V we investigate the correlations between the switch-on time, the chirp range, and the maximum intensity of the first intensity pulse.

II. INSTANTANEOUS FREQUENCY AND TRANSIENT SPECTRA

Several studies of frequency dynamics can be found in the literature [11–13, 17–19], but the precise meaning of

TABLE I. Meanings and values of the parameters in Eqs. (1)–(4) [16].

Parameter	Meaning	Value	Units
g	Gain parameter	5.6×10^4	s^{-1}
γ	Inverse photon lifetime	4×10^{11}	s^{-1}
γ_e	Inverse carrier lifetime	5×10^8	s^{-1}
C	Current injection	14×10^{16}	s^{-1}
N_0	Carrier number at transparency	6.8×10^7	adimensional
s	Inverse saturation intensity	1.25×10^{-6}	adimensional
α	Linewidth enhancement factor	5	adimensional
β	Spontaneous emission rate	1.1×10^4	s^{-1}
C_{th}	Threshold current	3.76×10^{16}	s^{-1}
C_{bias}	Bias current	3.4×10^{16}	s^{-1}

"instantaneous frequency" is rather elusive. It is clear from Eqs. (1)–(4) that in the absence of phase noise one can simply define the instantaneous angular frequency ω of the electric field as $\dot{\varphi}$. This approach has been widely used for analyzing communication systems [18], and it has been successful in the description of those systems which involve sinusoidal or pulsed modulation of the laser between a high-intensity and a low-intensity state. In this case, if the induced modulation of the laser is much larger than the spontaneous emission strength, the noise terms in Eqs. (1)–(4) can be neglected; this condition is more easily satisfied if the laser is always kept well above threshold, even in the low-intensity state, so that the phase noise strength is always small. Nevertheless, when spontaneous emission noise is not negligible, this definition is no longer meaningful. Although the mean value of ω ($\langle\dot{\varphi}\rangle$) is well defined, the standard deviation of ω around its mean value is infinite. This implies that there is equal probability of finding any particular value of ω in a single measurement, and that even in steady state the average of any finite subset of values may deviate substantially from the time average value.

This problem arises in both the steady state and the transient regime. It is associated with the nature of noise for the complex electric-field amplitude which underlies the stochastic rate equations and not with the strength of the phase noise, although the latter is larger along the transient due to the low values of the intensity. The infinite standard deviation of ω, which results from the white-noise property of δ-correlated noise sources, is an artifact of the approximations used to write the rate equations. Spontaneous emission of macroscopic devices is properly modeled as white noise in the electric dipole moment of the medium [27], which has been adiabatically eliminated to obtain the rate equations. The adiabatic elimination is based on the assumption that all time scales of evolution are much longer than the relaxation time for the polarization. At the very least, this procedure turns white noise in the polarization into colored noise (with its bandwidth limited by the polarization decay rate) for the electric field. Though the resulting noise has a correlation time much shorter than all other characteristic times of evolution of the remaining variables, it is only relatively white and the infinite standard deviation of the frequency is avoided in the exact expression. While a finite (but small) correlation time τ for the noise (colored noise) avoids the infinity, the standard deviation of ω around its mean value is very large ($\approx \tau^{-1}$), thereby masking any transient evolution. Hence $\dot{\varphi}$ generally lacks usefulness as a definition of a measurable instantaneous frequency in the presence of phase noise.

This does not contradict the idea that lasers are monochromatic, which is based not on direct frequency measurements but on field spectral power measurements [28]. In fact, the field spectrum provides the usual way to determine the steady-state laser frequency since most of the field spectral power is contained in a narrow frequency interval, yielding a well-defined peak in the field power spectrum. The frequency of the laser is taken to be the location of this peak, whose width is related to the noise strength. Unfortunately, if one wishes to study the frequency dynamics during a transient, the usual Fourier spectrum does not help since it involves the whole time evolution of the system. The Fourier components do not give information about the instantaneous frequency of the electric field.

Some hints for how to define an instantaneous frequency in the face of these limitations can be found by examining the procedure used for measuring it. One of the simplest and more common ways to study the frequency dynamics during the transient [11, 12] is to measure the power spectrum of the electric field by means of an interferometric device—which for simplicity we assume to be a grating monochromator. The output field produced by the diffraction grating at a given position is (in the far-field approximation)

$$E_d(\mathbf{r},t) = \sum_{m=1}^{M} E(t - m\tau)e^{i\Omega_c(t-m\tau)} , \tag{6}$$

where $\tau = \tau(\mathbf{r})$ is the time delay between rays coming from two consecutive rulings on the grating and M is the number of rulings. The diffracted intensity $I_d(\mathbf{r},t) = |E_d(\mathbf{r},t)|^2$ has maxima at different points which are assigned to different diffraction orders for the lasing frequency. Changes in the lasing frequency are detected as changes in the position of the maxima in the power spectrum. The low-frequency resolution of these measurements is limited by $(M\tau)^{-1}$, while the free spectral range $\approx (2\tau)^{-1}$ sets a high-frequency limit to the resolution. Note that the delays in the travel times from different rulings make such a measurement a partial time average.

Measurement with a monochromator is analogous to making a fast Fourier transform (FFT) of the incident electric field [29]. The time window for the equivalent FFT is $M\tau$, the total time difference between the extreme diffraction rulings, which yields a low-frequency resolution $(M\tau)^{-1}$, and the high-frequency resolution is given by the Nyquist frequency $(2\tau)^{-1}$. The limitations are just those of the time-frequency uncertainty principle. Decreasing the time window in order to have better temporal precision leads to a loss of frequency resolution. An increase in frequency resolution can be obtained only by letting the time window increase, but in this case we lose temporal information and all the Fourier components appear in the resulting spectrum. Therefore a compromise between the "instantaneousness" of the measured frequency and its accuracy has to be accepted.

While the field spectrum is the measurable quantity it would be useful if its characteristics could be understood in terms of the phase dynamics defined in Eqs. (1)–(4). Provided that during the transient the field amplitude is also varying in time, we expect two contributions to the spectrum, one arising from the field frequency itself and another one arising from the field amplitude evolution. Whether the movement of the maxima in the field power spectrum can be attributed only to frequency dynamics is not clear and is one of the reasons for our investigation.

In order to analyze this relationship we propose two approximately instantaneous frequencies which can be derived from Eqs. (1)–(4). We define the observable in-

stantaneous frequency (OIF) as

$$f_T(t) \equiv \frac{1}{2\pi T}\int_t^{t+T} d\tau\dot{\varphi}(\tau) , \quad (7)$$

where $\dot{\varphi}$ is given by Eq. (2), thereby including both phase noise directly and amplitude and carrier noise parametrically. To separate the role of the phase noise during the transient and its contributions to the laser frequency from the role of the amplitude and carrier noises, we define another frequency, analogous to the OIF but with phase fluctuations neglected,

$$F_T(t) \equiv \frac{1}{2\pi T}\int_t^{t+T} d\tau\frac{\alpha}{2}[G(\tau)-\gamma] , \quad (8)$$

which is the time average of the deterministic part of the equation for $\dot{\varphi}$. One should note that $F_T(t)$ is a random quantity since the gain G is a function of I and N which evolve stochastically according to Eqs. (1) and (3).

In these equations, T stands for the time window used for the FFT, and t for the time at which the measurement begins. The time averaging guarantees that the OIF defined by Eq. (7) always has a finite standard deviation around its mean value. This standard deviation increases as T decreases so that we lose precision as the time window is shortened.

These approximately instantaneous frequencies are useful for interpretations of the stochastic dynamics because of the following properties which are demonstrated in the following sections. The OIF corresponds to the time-dependent maximum of the FFT over short-time windows. It coincides with $F_T(t)$ when the laser intensity is large enough so that phase fluctuations can be neglected in comparison with $G-\gamma$ [see Eq. (2)].

III. ANALYSIS OF INDIVIDUAL SWITCH-ON EVENTS

Results for two different switch-on transients, A (solid line) and B (dashed line), obtained by numerical integration of Eqs. (1)–(4) are shown in Figs. 1, 2, and 3. In Figs. 1(a) and 1(b) we have plotted the laser intensity I and the carrier number N, respectively, versus time for these two transients. These results can be directly compared with those in Ref. [15] (calculated without gain saturation) in order to study the effects of the saturation term that we have included here. The effects of the gain saturation are twofold, it leads to a reduction of the maximum intensity reached in the relaxation oscillations and it decreases the number of relaxation oscillations. The same qualitative effects have been observed with different types of gain saturation [16, 30].

The growth of the carrier number—and hence the gain—is almost linear and deterministic until the laser switches on (the switch-on time t^* is defined as when the laser intensity becomes a chosen fraction of its final value) [2]. Therefore we find that the influence of the noise terms in the carrier number evolution is negligible unless the steady state is considered, in agreement with previous work [15, 16].

Finally, it can be seen that the later the switch-on time, the larger the maximum values of the carrier number and intensity. In addition, the minimum value of the carrier number after the first peak is lower for the trajectory with a larger overshoot of the intensity. Nevertheless, the difference in the minimum values of N is much smaller than the difference in the maximum values; this is a consequence of gain saturation which causes a clustering of the trajectories after the first intensity peak.

In Fig. 1(c) we have plotted $f \equiv (2\pi)^{-1}[\varphi(t+\Delta t)-\varphi(t)]/\Delta t$, which is the numerical approximation to the frequency that can be obtained with digitized data. It must be emphasized that the finite size of the fluctuations of f around its mean value is an artifact of the method of integration due to the finite size of the integration step Δt. In fact, as $\Delta t \to 0$ the size of the fluctuations diverges. Nevertheless, provided that the fluctuations at any time are scaled in exactly the same way, they are representative of the real process. As a consequence, we can see that there is a noise-dominated regime for f, corresponding to times before t^*. Moreover, two different stages can be distinguished in the noisy regime. The first one corresponds to times before the threshold time $t_{\rm th}$=67.4 ps, which is the time at which N reaches its threshold value. In this time interval, noise contributions to phase dynamics are huge and dominant. For times t such that $t_{\rm th} < t < t^*$, phase noise contributions are

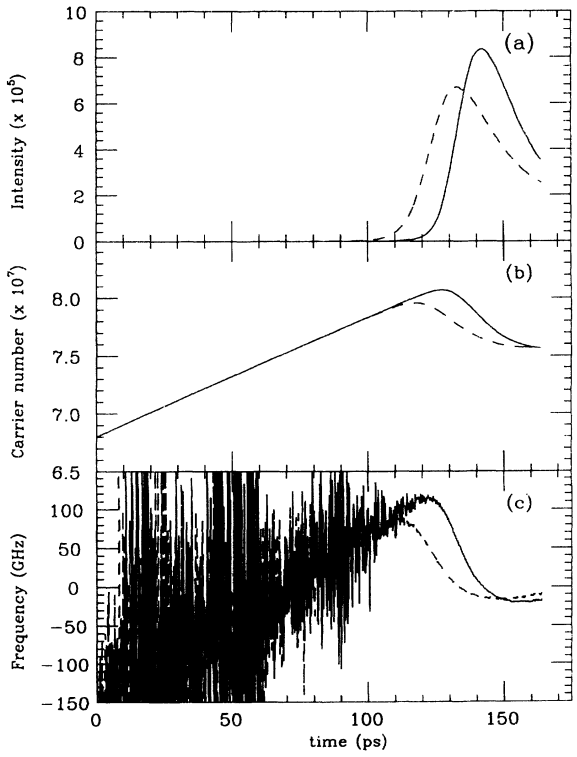

FIG. 1. Time evolution of (a) intensity, (b) carrier number, and (c) frequency $f \equiv (2\pi)^{-1}\Delta\varphi/\Delta t$ as obtained from the numerical simulation of Eqs. (1)–(4) for two different switch-on transients: A (solid line) and B (dashed line). The switch-on times (where the intensity first crosses 1% of its final value) are $t^* \sim 120$ and 105 ps for transients A and B, respectively.

still important, but they are progressively reduced as the intensity grows.

The randomness of the frequency chirp in the transient can also be observed in Fig. 1(c). When the intensity switch-on is later, the chirp is larger. This dependence stems from the fact that the maximum carrier number (and hence the maximum deterministic gain) increases as the switch-on time increases. Therefore, the maximum value of f in the region of measurable intensity, which roughly corresponds (except for fluctuations) to the maximum deterministic gain, also increases. The minimum value of f which comes after the first peak in the intensity is much less sensitive to the switch-on time due to the clustering of the trajectories for the intensity and carrier number caused by gain saturation and the resulting strong damping of the relaxation oscillations.

In Figs. 2 and 3 we have plotted different field power spectra for each transient, calculated over different time windows for the FFT. The plots in Fig. 2 correspond to taking the time window equal to the whole time interval studied (T=163.84 ps). As already noted, this time interval is so large that we lose information about the temporal variation in the instantaneous frequency of the electric field; we obtain a broad spectrum with contributions from all the field frequency components. We expect the overall width of the spectrum to correspond to the range of the frequency chirp. The spectra have the shape of a plateau with higher power concentrated in the low-frequency side. This asymmetry in the power spectrum arises from the evolving field amplitude, since the high-frequency range corresponds to times close to t^*, where the intensity has not yet reached a large value. We observe that the trajectory with later intensity growth presents a wider spectrum, which can be understood as the signature of a larger frequency chirp [compare with Fig. 1(c)].

This same conclusion can also be drawn from spectra taken over shorter time windows, such as those in Fig. 3. These spectra have been calculated by dividing the total time interval into eight nonoverlapping intervals of length T=20.48 ps, so the frequency resolution is $\approx \pm 25$ GHz. The power in the FFT for each trajectory in each of these time intervals is plotted. It can be seen that the variations in the positions of the maxima in the power spectra are larger for the trajectory growing later, thus indicating a larger frequency chirp, but the limited frequency resolution prevents precise measurements. The half-width at half maximum (HWHM) for each of these spectra stays more or less constant for the first five intervals and then it decreases to lower values, though once again a precise quantitative measurement is not possible because of limited frequency resolution.

The vertical solid (dashed) line in Fig. 3 corresponds to the value of the OIF for transient A (B) on each time interval. Its position corresponds to the maximum of the power spectrum for each window of time and for each transient. Therefore the OIF defined in Eq. (7) accurately represents the evolution of the maximum in successive short-time spectra. The frequency $F_T(t)$ is not as accurate for times before the switch-on time. For comparison, we list in Tables II and III the values of $f_T(t)$ and $F_T(t)$ for transients A and B, respectively. We see that there are substantial differences for times $t \leq 81.92$ ps, and that for $t > 102.40$ ps, the two frequencies coincide. Therefore, we again encounter the two different regimes for the frequency already discussed, namely, times earlier or later than the switch-on time t^* [compare with

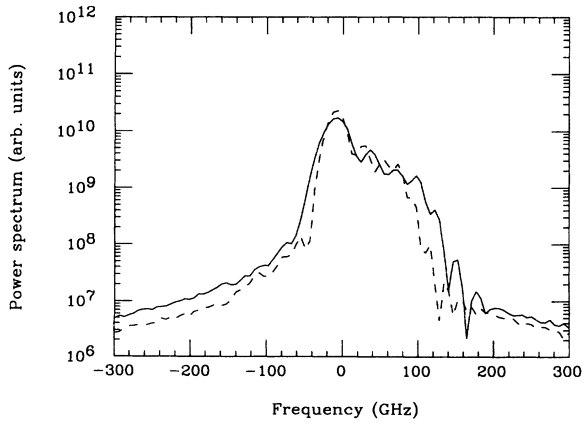

FIG. 2. Power spectrum for the switch-on transients in Fig. 1, obtained by the FFT of the electric field over the total time interval T = 163.84 ps.

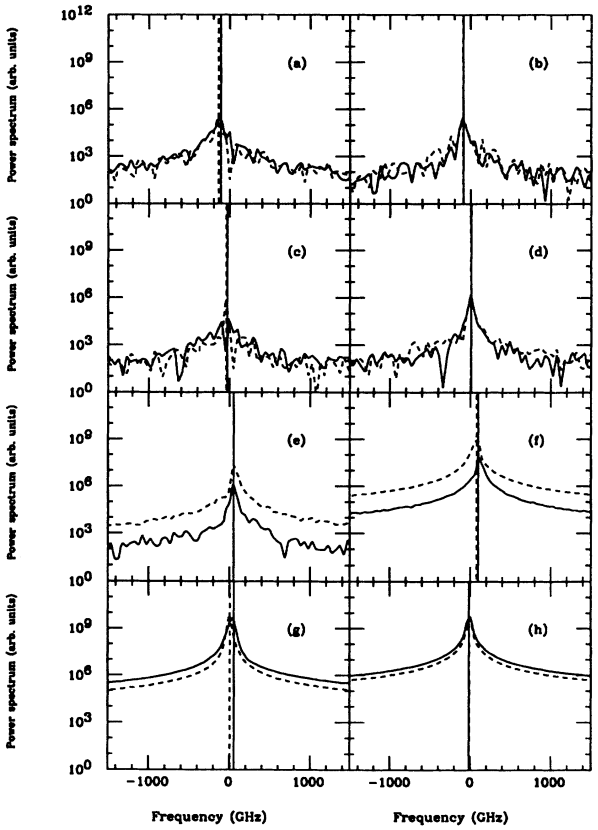

FIG. 3. Power spectra for the switch-on transients in Fig. 1, obtained by the FFT of the electric field over a short-time window (T = 20.48 ps), and starting at times (a) 0 ps, (b) 20.48 ps, (c) 40.96 ps, (d) 61.44 ps, (e) 81.92 ps, (f) 102.40 ps, (g) 122.88 ps, and (h) 143.36 ps.

TABLE II. Values of $f_T(t)$ and $F_T(t)$ on each time interval for transient A (see text).

t (ps)	T (ps)	$f_T(t)$ (GHz)	$F_T(t)$ (GHz)
0.00	20.48	−107.77	−135.05
20.48	20.48	−88.49	−87.16
40.96	20.48	−27.34	−39.80
61.44	20.48	6.46	7.06
81.92	20.48	54.54	53.46
102.40	20.48	97.92	97.62
122.88	20.48	55.31	55.27
143.36	20.48	−16.73	−16.74

Fig. 1(c)]. The sixth time interval [Fig. 3(f), t=102.40 ps] contains the switch-on time for both trajectories [see Fig. 1(a)], and after this time $f_T(t)$ and $F_T(t)$ coincide. This, along with the reduction in linewidth of the spectra, is a clear indication that phase fluctuations in this time interval play a secondary role. In fact, due to the rapid growth of the intensity, the phase noise strength is strongly reduced and, in these time intervals, the phase evolves as a deterministic function of I and N.

IV. STATISTICS

Two thousand switch-on events corresponding to Eqs. (1)–(4) have been numerically calculated. Results for the averaged intensity $\langle I \rangle$ and carrier number $\langle N \rangle$ are shown in Fig. 4 along with their standard deviations around their means. In comparison with the results of Ref. [15], where no gain saturation was considered, the gain saturation reduces the maximum intensity reached during the relaxation oscillations, and it reduces the peak of the fluctuations of the intensity. This peak is a well-known feature of transient dynamics and is referred to as "anomalous intensity fluctuations [1–3]." However, the anomalous fluctuations are not affected by gain saturation during the transient until the intensity reaches a macroscopic value; earlier, they coincide with the case without gain saturation. This is not surprising since it has been well established [1,2] that the anomalous fluctuations appear as a consequence of the randomness in the distribution of switch-on times. Provided that gain saturation in the initial regime is not important ($sI << 1$),

TABLE III. Values of $f_T(t)$ and $F_T(t)$ on each time interval for transient B (see text).

t (ps)	T (ps)	$f_T(t)$ (GHz)	$F_T(t)$ (GHz)
0.00	20.48	−139.83	−135.08
20.48	20.48	−93.02	−87.26
40.96	20.48	−41.71	−39.88
61.44	20.48	2.72	7.02
81.92	20.48	53.86	53.03
102.40	20.48	75.83	76.33
122.88	20.48	5.49	5.45
143.36	20.48	−13.83	−13.75

the intensity fluctuations are not affected by the inclusion of the saturation term until times later than the switch-on time.

For each trajectory we have calculated nine field power spectra by means of a FFT: one covering the whole time window studied (overall spectrum, T = 163.84 ps) and eight short-time spectra (eight nonoverlapping intervals of length T=20.48 ps).

The averaged overall spectrum is plotted using a solid line in Fig. 5, and it shows contributions above the noise level only for frequencies ranging from ≈ -20 to ≈ 100 GHz, which can be taken as an estimate of the average chirp range. Outside this interval, the spectral power drops several orders of magnitude in a narrow frequency range.

We have already noted the asymmetric form of the central portion of the power spectra of the individual transients, assigning it to the evolving field amplitude. In addition, the wings of the average power spectrum are more asymmetric, and the high-frequency wing decreases to the noise level in a smoother way than the low-frequency wing. This reflects the fact that the dispersion in the maximum frequency reached along each trajectory is much larger than the dispersion of the minimum frequency. Once again, this is a consequence of the evolving field intensity, since the maximum frequency is reached at approximately the switch-on time, when the intensity is small and saturation effects are not yet important, so that the relatively small fluctuations of t^* induce larger frequency fluctuations. In contrast, the minimum frequency is obtained after the first intensity peak, where the clustering of the trajectories induced by the gain saturation strongly reduces the fluctuations due to the different switch-on times (compare with the results in Ref. [15]). Therefore the fall of the power spectrum on the low-frequency side is much sharper than the fall on the high-frequency side, and this asymmetry in both the spectrum and its wings prevents a simple definition of the chirp range in terms of the full width at half maximum of the power spectrum.

The stochastic character of the chirp range can also be clearly seen in Fig. 5, where we have plotted, using a dash-dotted line, the relative power fluctuation R at each frequency,

$$R \equiv \left(\frac{\langle |E(f)|^4 \rangle}{\langle |E(f)|^2 \rangle^2} - 1 \right)^{1/2} ,$$

$E(f)$ being obtained from the FFT of the electric field. These fluctuations are essentially constant except for two narrow frequency intervals corresponding to the sudden falls in the averaged power spectrum. The R reaches maximum values at $f_{\min} \approx -50$ GHz and $f_{\max} \approx 100$ GHz. For these frequencies, large relative fluctuations are observed which describe the important differences in the contributions to the power spectrum from different trajectories, and hence the stochastic nature of the chirp range. Also, the peak on the low-frequency side is much narrower than the peak on the high-frequency wing, in agreement with the previous discussion.

In Fig. 6 we have plotted the average of the short-

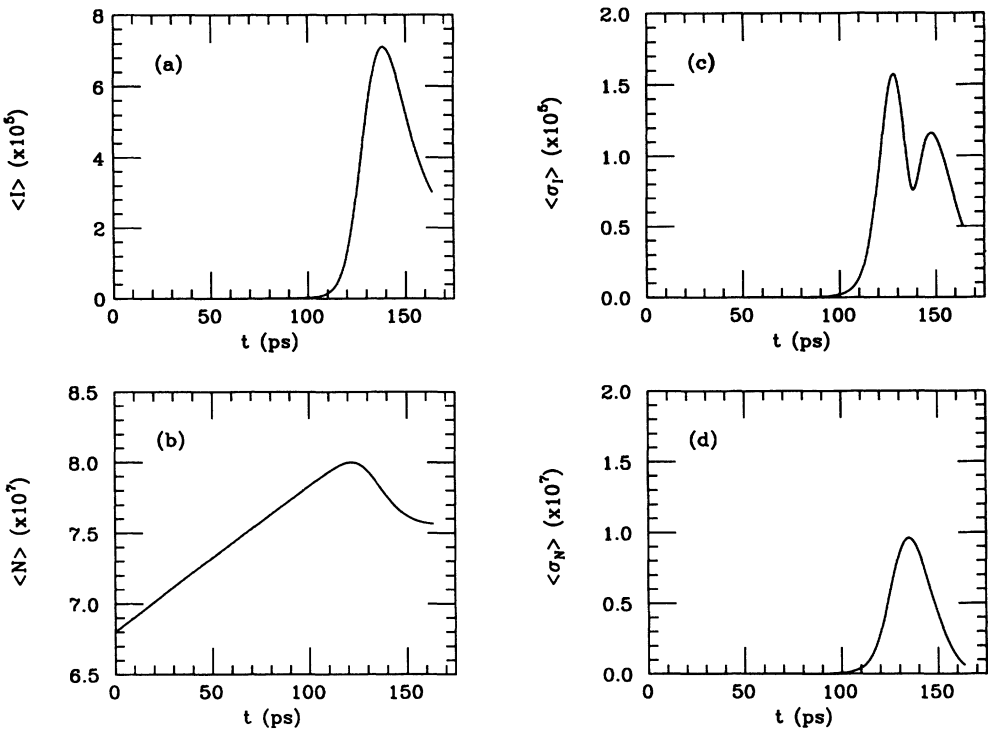

FIG. 4. Time evolution of (a) mean intensity, (b) mean carrier number, (c) standard deviation of the intensity, and (d) standard deviation of the carrier number, as obtained from the numerical simulation of Eqs. (1)–(4) for 2000 switch-on transients.

time spectra. The position of the maximum in the power spectrum for each time interval clearly shifts back and forth, thus indicating the frequency variation along the transient. The largest peak frequency is obtained in the sixth interval (ranging from t=102.4 to 122.88 ps), reaching $\approx$ 100 GHz. The smallest frequency is ≈ -150 GHz, and it appears in the first time interval, taken from t=0 to 20.48 ps. Hence, this smallest frequency corresponds to the smallest value of the carrier number at t=0, and not to the local minimum value reached during the relaxation oscillations. Comparison of these results for the short-time spectra with those of the overall spectrum re-

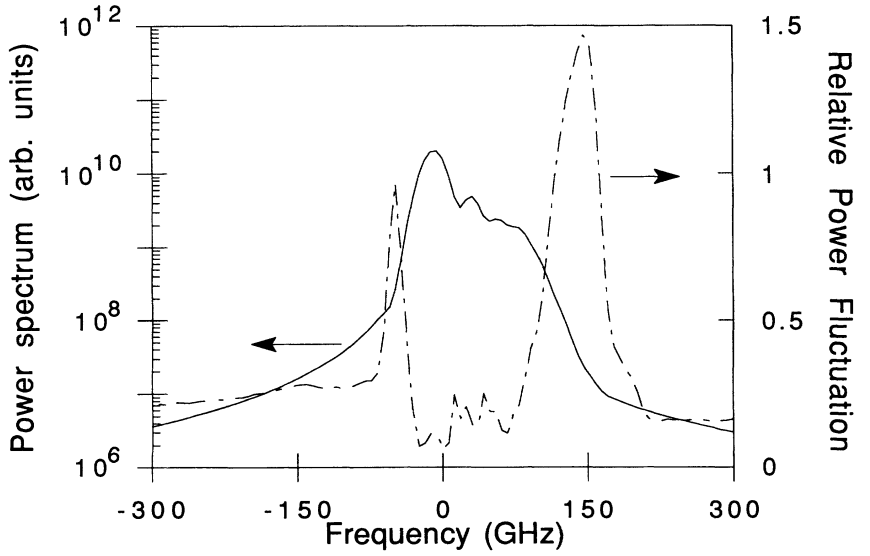

FIG. 5. Average power spectrum (PS, solid line) and relative power fluctuation (R, dashed line). The PS and R are obtained by averaging over the 2000 transients the results for the spectral power in the FFT of the electric field over the total time interval T = 163.84 ps.

veals that the largest frequencies in the two cases coincide within our frequency resolution. However, the results for the smallest frequencies are very different. The discrepancy is due to the huge differences in spectral power between those frequencies, since the spectral power corresponding to the smallest frequency in the short-time window spectra is three orders of magnitude lower than the spectral power corresponding to the largest frequency. The local minimum frequency with spectral power within one order of magnitude of that of the maximum frequency appears in the last time interval, after the first intensity peak, and it is located between 0 and −50 GHz. Therefore, the large-time window spectrum detects only the lowest frequency after the first peak of the intensity, neglecting the low-frequency components present at earlier very low intensities, and as a consequence it reflects only the quasilinear sweep of the frequency along the first intensity peak, i.e., the chirp range.

For studying the extent to which these spectra can be understood in terms of the frequency dynamics defined by Eqs. (1)–(4), and to discern the phase noise contributions to the spectra, we have calculated the mean values of $f_T(t)$ [Eq. (7)] and $F_T(t)$ [Eq. (8)], as well as their standard deviations from these mean values. The results are shown in Fig. 7. The mean values of the two frequencies are nearly coincident, and yield a minimum frequency of −135 GHz at $t = 0$ (−17 GHz at $t = 143.36$ ps) and a maximum frequency of 90 GHz at $t = 102.4$ ps. These values are quite similar to those obtained from the short-time spectra for each interval. The agreement is shown in Fig. 6, where the dotted vertical line indicates the averaged value of the OIF $f_T(t)$.

The differences between the frequencies $f_T(t)$ and $F_T(t)$ are evident in their standard deviations. $f_T(t)$ has a large standard deviation around its mean for times before the mean switch-on time ($\langle t^* \rangle \sim 100 - 120$ ps). The standard deviation has a maximum at $t = 20.48$ ps, and then it decreases continuously until $\langle t^* \rangle$. This maximum may be an artifact of the procedure used, since we start our simulations from a fixed initial condition of (nearly) zero intensity, and so we do not consider the fluctuations in the initial condition. As a consequence, we underestimate the deviations from the mean value in the first time interval, so the maximum may disappear when they are accounted for, although we believe that it does not affect the discussion about the definition of an instantaneous frequency. In contrast, $F_T(t)$ has a very small standard deviation around its mean until $\langle t^* \rangle$, where it suddenly increases and, from this time on, the fluctuations of both frequencies are equal. Comparison with the linewidths (taken as the HWHM) of the short-time spectra clearly establishes that the OIF, $f_T(t)$, gives a close approximation to these spectra, while $F_T(t)$ yields unrealistic linewidths for times before $\langle t^* \rangle$.

An *a priori* criterion for choosing one frequency or the other, in the sense of determining which one yields a realistic linewidth, is usually provided by the field-field correlation function $C(t_1, t_2) \equiv \langle E(t_1) E^*(t_2) \rangle$. For a correlation function which decreases exponentially with the time difference $|t_1 - t_2|$, the HWHM corresponds to the inverse of the correlation time deduced from the field-field correlation function divided by 2π. In the present case, the correlation function can be explicitly calculated

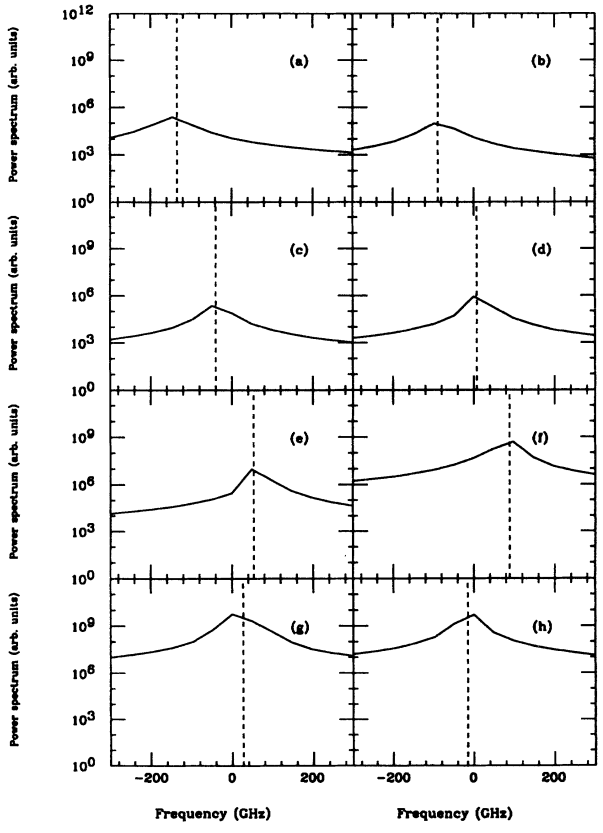

FIG. 6. Power spectra averaged over the 2000 transients obtained by the FFT of the electric field over a short-time window ($T = 20.48$ ps), and starting at times (a) 0 ps, (b) 20.48 ps, (c) 40.96 ps, (d) 61.44 ps, (e) 81.92 ps, (f) 102.40 ps, (g) 122.88 ps, and (h) 143.36 ps. The dashed vertical line shows the averaged value of the OIF, $f_T(t)$, defined by Eq. (7).

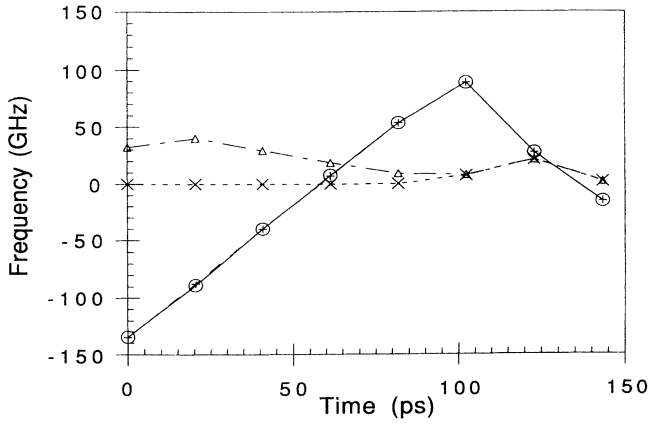

FIG. 7. Mean values of the frequencies $f_T(t)$ (o) and $F_T(t)$ (+) defined by Eqs. (7) and (8), respectively. Also plotted are the standard deviations of $f_T(t)$ (△) and $F_T(t)$ (×). The starting times t and the time window T correspond to those used in the calculation of the short-time spectra. Lines are guides to the eye.

for times t_1, $t_2 < t^*$. In this time interval the intensity is very small, so saturation effects are not important, and since the carrier number is quite far away from its steady-state value, noise terms in Eq. (3) can be neglected. In addition, it is obvious that in this time regime phase noise will be important. With these approximations, Eqs. (1)–(4) can be rewritten as

$$\dot{E} = \frac{1+i\alpha}{2}\left[g(N-N_0)-\gamma\right]E + \sqrt{\beta N}\xi(t)\ , \tag{9}$$

$$\dot{N} = C - \gamma_e N\ , \tag{10}$$

where $E = \sqrt{I}e^{i\varphi}$ is the complex amplitude of the electric field. $\xi(t) = \xi_1(t) + i\xi_2(t)$ is a complex Gaussian white noise of zero mean and correlations given by

$$\langle \xi_i(t)\xi_j(t')\rangle = 2\delta_{ij}\delta(t-t')\ ,\quad i,j = 1,2\ . \tag{11}$$

The solution to Eqs. (9) and (10) then reads

$$N(t) = N(0)e^{-\gamma_e t} + \frac{C}{\gamma_e}(1-e^{-\gamma_e t})\ , \tag{12}$$

$$E(t) = e^{A(t)/2}\ h(t)\ , \tag{13}$$

$$A(t) = (1+i\alpha)\int_0^t dt'\left\{g\left[N(t')-N_0\right]-\gamma\right\}\ , \tag{14}$$

$$h(t) = E(0) + \int_0^t dt'\sqrt{\beta N(t')}\xi(t')e^{-A(t')/2}\ , \tag{15}$$

where $E(0)$, $N(0)$ stand for the initial values of the electric field and the carrier number, respectively. In the simulations we have considered $E(0) \simeq 0$, and now we can calculate the field-field correlation function. Taking into account that for all times of interest $\gamma_e t << 1$, after some algebra we find

$$C_x(y) = 4\beta\ e^{i2\alpha xy}\ e^{x^2+y^2}\ \{k_1[\mathrm{erf}(x-|y|)+\mathrm{erf}(\lambda)] + k_2(e^{-\lambda^2} - e^{-(x-|y|)^2})\}\ , \tag{16}$$

where $\mathrm{erf}(x)$ stands for the error function [31] and we have defined $x \equiv (\mu/2)^{1/2}(t_1+t_2-2\bar{t})/2$, $y \equiv (\mu/2)^{1/2}(t_1-t_2)/2$, $\lambda \equiv (\mu/2)^{1/2}\bar{t}$, $\mu \equiv g[C-\gamma_e N(0)]$, $\bar{t} \equiv \{g[N_0-N(0)]+\gamma\}/\mu$, $k_1 \equiv (\pi/2\mu)^{1/2}(N_0+\gamma/g)$ and $k_2 \equiv g^{-1}$.

This correlation function presents a very interesting behavior, as depicted in Fig. 8, where we have plotted $|C_x(y)|$, normalized to its value at $t_1 = t_2$, $|C_x(0)|$, as a function of y, keeping constant x. For short times [Figs. 8(a) ($x=-3$), 8(b) ($x=-2$), and 8(c) ($x=-1$)], the maximum modulus of the field-field correlation function appears at $y = 0$. For increasing time difference, the correlation decreases quite rapidly, in a fashion that closely resembles a decreasing exponential of the time difference, as can be seen from the linear behavior of $|C_x(y)|$. The exponential loss of correlation for increasing time differences indicates that, in this time interval, the evolution of the electric field is dominated by noise. Nevertheless, as one of the times is allowed to reach the switch-on time [Fig. 8(d) ($x=0$) for $y \gtrsim 2.5$], an increase in the field-field correlation is observed. This is due to the buildup of the electric field from the spontaneous emission, which leads to noise amplification and, as a consequence, to increasing correlation among fields at different times. For greater x [Figs. 8(e)–8(g)], the field-field correlation increases faster than a simple exponential for moderate values of y, this being the signature of deterministic amplification of the spontaneous emission.

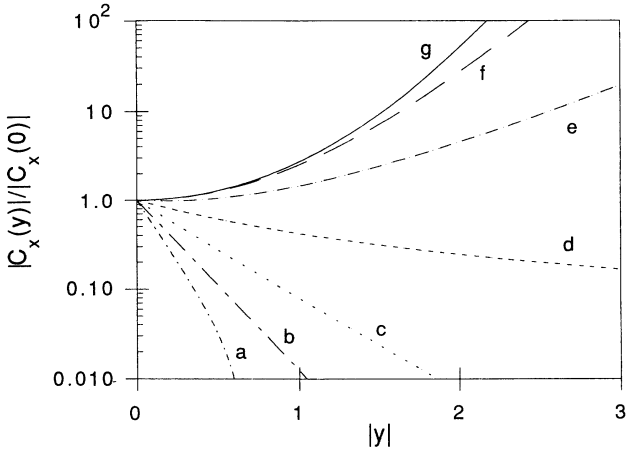

FIG. 8. Field-field correlation function for times before t^*, normalized to its value at $y = 0$ (i. e., at equal times): (a) $x = -3$, (b) $x = -2$, (c) $x = -1$, (d) $x = 0$, (e) $x = 1$, (f) $x = 2$, and (g) $x = 3$.

The complicated dependence on the time difference (y) prevents us from taking a simple definition for the linewidth in terms of the correlation time. Nevertheless, we can estimate the linewidth and its behavior by considering the time difference necessary for reducing (or increasing) the modulus of the correlation function by a factor of 2 with respect to its value at zero time difference. With this definition, we obtain correlation times of 4.25, 6.4, 10.6, 27.6, 51, 33.15, and 31 ps for curves a–g, respectively, which correspond to linewidths (defined as the inverse correlation time divided by 2π) of 37, 25, 15, 6, 3, 5, and 5 GHz, respectively. Though the identification of this quantity with the standard deviation in the OIF is quite arbitrary, the general trend in both cases is the same (compare with Δ in Fig. 7): it decreases from a high value to a minimum and then increases again, being always of the order of several GHz. In contrast, the behavior of the standard deviation of $F_T(t)$ is completely different, so the inverse correlation time compares much better with the standard deviation of $f_T(t)$ than with that of $F_T(t)$. The good agreement persists throughout the domain of validity of $C_x(y)$ ($t, t' < t^*$) and even continues for somewhat larger times.

The different behavior of the standard deviations of the two frequencies [Eqs. (7) and (8)] is a clear signature of the influence of phase noise on the dynamics of the system, and we can distinguish the two different regions along the transient previously noted. In the first one, ranging from $t = 0$ to $t = \langle t^* \rangle$, the laser linewidth is dominated by phase fluctuations. As time increases, the growing intensity makes phase fluctuations less important and for $t > \langle t^* \rangle$ the transient anomalous fluctuations

determine the laser linewidth.

Finally, in order to obtain a better determination of the chirp range, we have calculated the maximum value of $f \equiv (2\pi)^{-1}\Delta\varphi/\Delta t$ in the region of measurable intensity, as well as the minimum value of f after this maximum, for each trajectory. Averaging, we obtain a maximum frequency $\langle f_{\max}\rangle = 99.0$ GHz with a standard deviation of 10.1 GHz. The minimum frequency obtained in this way is $\langle f_{\min}\rangle = -17.8$ GHz with a standard deviation of 1.4 GHz. These results are in good agreement with those obtained from the average of the spectra taken for the total time interval. Very similar results are obtained by averaging the maximum and minimum values of $(4\pi)^{-1}\alpha(G-\gamma)$, thus confirming that the chirp range is nearly independent of the phase noise. The reason is that at the peak the intensity reaches such high values that the phase noise strength is very small, hence the frequency in this time interval behaves like a deterministic function of the variables I and N.

V. CONNECTION BETWEEN CHIRP RANGE AND SWITCH-ON TIME

From the previous analysis it is clear that the laser frequency at the first peak of the intensity is determined by the gain, and that phase noise is not important in this time interval. The deterministic dependence of the frequency on the random variables I and N then establishes the chirp range for each trajectory. These two variables form a closed system whose evolution has been shown [15, 16] to be properly described by a quasideterministic approximation [32] which allows us to successfully explain different aspects of the transient dynamics of this system. In particular, it has been shown in Refs. [15] and [16] that after the switch-on time, the role of the spontaneous emission noise in the evolution of I and N can be modeled by a random effective initial condition. Since in this time interval the frequency can be taken as a deterministic function of both the intensity and carrier number, which in turn can be understood as deterministic functions of a random variable (either the random initial condition or the first passage time), we expect a close relation between the frequency chirp range and the switch-on time for each trajectory.

We have investigated this possibility, taking the chirp range to be $f_{\max}-f_{\min}$, where $f_{\max}$ and $f_{\min}$ stand for the maximum and minimum values of the frequency in the region of measurable intensity. The results are shown in Fig. 9, where we have plotted the chirp range versus the first passage time t^* for each trajectory for different values of the reference intensity [$I_r = 1000$ (•), 5000 (o), and 10000 (×)]. These values amount to ≈ 0.4%, 2%, and 4%, respectively, of the asymptotic steady-state value of the intensity. A linear relation between the chirp range and t^* holds to good approximation, although some scattering of the data is evident. The scattering is reduced as the reference value for the intensity is increased, and for $I_r = 10000$ it is already nearly negligible. As a consequence, for reasonably small values of the reference intensity, there is a linear relationship between t^* and the chirp range. The chirp range for each trajectory increases linearly with the switch-on time. Hence, the statistical properties of the distribution of chirp ranges can be immediately deduced from those of the first-passage-time distribution.

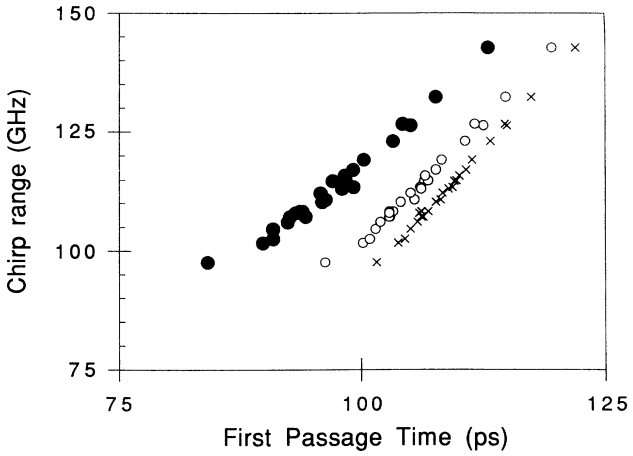

FIG. 9. Chirp range vs first passage time for different values of the reference intensity: $I_r = 1000$ (•), $I_r = 5000$ (o), and $I_r = 10000$ (×), which correspond to ≈ 0.4%, 2%, and 4% of the final steady-state value, respectively.

On the other hand, it has been shown that in the absence of gain saturation the maximum peak intensity depends linearly on the first passage time [15]. Since it is not clear to what extent this result depends on gain saturation, we have checked this relation in the present case. The results are plotted on Fig. 10, and it can be seen that a linear relation between the maximum peak intensity and t^* is still obtained. The slope is positive, but it is much smaller than in the case without saturation, indicating that the slope strongly depends on the saturation parameter s.

The deterministic relation between chirp range, maximum peak intensity, and first passage time implies that the chirp range has to be reduced by increasing the sat-

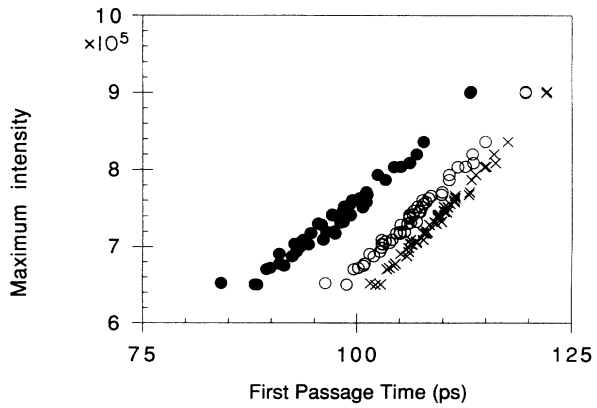

FIG. 10. Maximum value of the intensity during the first peak of the relaxation oscillations vs first passage time for different values of the reference intensity: $I_r = 1000$ (•), $I_r = 5000$ (o), and $I_r = 10000$ (×), which correspond to ≈ 0.4%, 2%, and 4% of the final steady-state value, respectively.

uration parameter, in agreement with experimental observations [13]. In addition, it permits a variety of practical applications in which the selection of one of these three variables automatically fixes the values of the others. Hence a single discriminator set to select pulses of a particular delay time (particular pulse height) automatically acts to select a subset of pulses with a particular chirp range and a particular pulse height (delay time).

VI. SUMMARY AND CONCLUSIONS

We have studied the frequency dynamics of single-mode semiconductor laser transients. We have discussed different ways to analyze and explain the changes in the approximately instantaneous frequency of the electric field and their relation to the experimentally measured spectra. We have shown that experimental optical power spectra for a single transient can be explained in terms of the OIF, $f_T(t)$, defined in Eq. (7). The changes of the maximum in the field FFT power spectrum taken over relatively short-time intervals correspond to the frequency dynamics of the OIF which is governed by Eqs. (1)–(4). When the power spectrum is taken over time windows long enough to include the first peak of the intensity, the width of the spectrum corresponds to the chirp range during the peak.

The influence of phase noise during the transient has been explored, and we find that it is not important during the first intensity peak. In this time interval, $f_T(t)$ and $F_T(t)$ coincide because the intensity reaches such a high value that the phase noise strength in (3) is negligible in comparison with the deterministic drift of $\dot{\varphi}$. As a consequence, the chirp range during this pulse is essentially independent of phase noise. Nevertheless, since the frequency of the electric field becomes a deterministic function of the laser intensity and the carrier number, the chirp range is a stochastic variable. The randomness of the chirp range is specially evident in the relative power fluctuation of spectra taken over long-time windows. It is also manifest in the short-time window spectra, but in this case the poor frequency resolution makes it difficult to detect. As a consequence of the randomness of the chirp range, the spectral properties of a single transient can differ appreciably from the average spectral characteristics.

Finally, we have studied the correlations between the chirp range and the first passage time for each transient. A linear dependence of the chirp range on the first passage time is demonstrated. In addition, the maximum intensity of the first pulse during the relaxation oscillations is linearly correlated with the switch-on time. The correlations permit a single discriminator to select a subset of pulses with similar peak intensities, delay times, and chirp ranges.

ACKNOWLEDGMENTS

Financial support from the Comisión Interministerial de Ciencia y Tecnología, Project No. TIC90/080 is acknowledged. We gratefully acknowledge the National Science Foundation for support of supercomputing services provided through the National Center for Supercomputing Applications.

* Present address: Physics Department, Bryn Mawr College, Bryn Mawr, PA 19010-2899.

† Permanent address: Dipartimento di Fisica, Università di l'Aquila, L'Aquila, I-67100, Italy.

‡ Permanent address: Physics Department, Bryn Mawr College, Bryn Mawr, PA 19010-2899.

[1] F.T. Arecchi, V. Degiorgio, and B. Querzola, Phys. Rev. Lett. **19**, 1168 (1967); M. Sargent, M. O. Scully, and W. E. Lamb, Appl. Opt. **9**, 2423 (1970); D. Meltzer and L. Mandel, Phys. Rev. Lett. **25**, 1151 (1970); F.T. Arecchi and V. Degiorgio, Phys. Rev. A **3**, 1108 (1971); F. Haake, J.W. Haus, and R. Glauber, *ibid.* **23**, 3255 (1981); R. Roy, A. W. Yu, and S. Zhu, Phys. Rev. Lett. **55**, 2794 (1985); Phys. Rev. A **34**, 4333 (1986); F. de Pasquale, J. M. Sancho, M. San Miguel, and P. Tartaglia, Phys. Rev. Lett. **56**, 2473 (1986); F. T. Arecchi, in *Noise and Chaos in Nonlinear Dynamical Systems*, edited by F. Moss, L. Lugiato, and W. Schleich (Cambridge University Press, Cambridge, 1990), p. 261.

[2] For a review on laser statistics, see, for instance, M. San Miguel, in *Laser Noise*, edited by R. Roy, SPIE Proc. No. 1376 (Bellingham, 1991), p. 272.

[3] F.T. Arecchi, R. Meucci, and J.A. Roversi, Europhys. Lett. **8**, 225 (1989); F.T. Arecchi, W. Gadomski, R. Meucci, and J.A. Roversi, Phys. Rev. A **39**, 4004 (1989); Opt. Commun. **65**, 47 (1988).

[4] M. Lefebvre, P. Bootz, D. Dangoisse, and P. Glorieux, in *Laser Spectroscopy VI*, edited by H.P. Weber and W. Lüthy (Springer-Verlag, Heidelberg, 1983), p. 282; P. Glorieux and D. Dangoisse, in *Handbook of Molecular Lasers*, edited by P.K. Cheo (Dekker, New York, 1987), pp. 573–644 (specifically pp. 615–617).

[5] M.C. Torrent and M. San Miguel, Phys. Rev. A **38**, 245 (1988).

[6] C.O. Weiss, N.B. Abraham, and U. Hübner, Phys. Rev. Lett. **61**, 1587 (1988); H. Zeghlache, P. Mandel, N.B. Abraham, and C.O. Weiss, Phys. Rev. A **38**, 3128 (1988); H. R. Telle, D. Meschede, and T.W. Hänsch, Opt. Lett. **15**, 532 (1990).

[7] S. Ciuchi, M. San Miguel, N. B. Abraham, and F. de Pasquale, Phys. Rev. A **44**, 7657 (1991); S. Ciuchi, F. de Pasquale, M. San Miguel, and N. B. Abraham, in *Nonlinear Dynamics in Optical Systems*, edited by N. B. Abraham, E. Garmire, and P. Mandel (Optical Society of America, Washington, DC, 1991), p. 428.

[8] F. T. Arecchi, G. L. Lippi, G. P. Puccioni, and J. R. Tredicce, Opt. Commun. **51**, 308 (1984).

[9] C. H. Henry, IEEE J. Quantum Electron. **QE-18**, 259 (1982).

[10] G. P. Agrawal and N. K. Dutta, *Long-Wavelength Semiconductor Lasers* (van Nostrand Reinhold, New York, 1986).

[11] S. Kobayashi, Y. Yamamoto, M. Ito, and T. Kimura, IEEE J. Quantum Electron. **QE-18**, 582 (1982); G. Mo-

tosugi, Y. Yoshikuni, and Y. Itaya, Electron. Lett. **18**, 849 (1984); Y. Suematsu, S. Arai, and F. Koyama, Opt. Acta **32**, 1157 (1985); C. Lin, G. Eisenstein, C. A. Burrus, and R. S. Tucker, Appl. Phys. Lett. **46**, 12 (1985); J. O'Gorman, A. F. J. Levi, T. Tanbun-Ek, and R. A. Logan, *ibid.* **58**, 669 (1990).

[12] Y. Yoshikumi, T. Matsukoa, G. Motosugi, and N. Yamanaka, Appl. Phys. Lett. **45**, 820 (1984); N. Henmi, S. Fujita, M. Yamaguchi, M. Shikada, and I. Mito, IEEE J. Lightw. Tech. **8**, 936 (1990).

[13] R. A. Linke, Electron. Lett. **20**, 472 (1984); IEEE J. Quantum Electron. **QE-21**, 593 (1985).

[14] P. Spano, A. D'Ottavi, A. Mecozzi, and B. Daino, Appl. Phys. Lett. **52**, 2203 (1988); A. Mecozzi, S. Piazzolla, A. D'Ottavi, and P. Spano, Phys. Rev. A **38**, 3136 (1988); A. D'Ottavi, A. Mecozzi, P. Spano, and S. Piazzolla, Appl. Phys. Lett. **53**, 2362 (1988); P. Spano, A. D'Ottavi, A. Meccozzi, B. Daino, and S. Piazzolla, IEEE J. Quantum Electron. **25**, 1440 (1989).

[15] S. Balle, P. Colet, and M. San Miguel, Phys. Rev. A **43**, 498 (1991).

[16] A. Mecozzi, P. Spano, and A. Sapia, Opt. Lett. **15**, 1067 (1990); P. Spano, A. Mecozzi, and A. Sapia, Phys. Rev. Lett. **64**, 3003 (1990); A. Czylwok and W. Eberle, IEEE J. Quantum Electron. **26**, 225 (1990).

[17] G. P. Agrawal, *Nonlinear Fiber Optics* (Academic, San Diego, 1989), Chap. 6 and references therein.

[18] K. Kishino, S. Aoki, and Y. Suematsu, IEEE J. Quantum Electron. **QE-18**, 343 (1982); D. Marcuse, *ibid.* **QE-19**, 1397 (1983); T. L. Koch and J. E. Bowers, Electron. Lett. **20**, 1039 (1984); J. Buus, *ibid.* **21**, 129 (1985); F. Koyama and Y. Suematsu, IEEE J. Quantum Electron. **QE-21**, 292 (1985); A. S. Sudbø, *ibid.* **QE-23**, 1127 (1987); G. P. Agrawal and C. H. Henry, *ibid.* **24**, 134 (1988).

[19] K. Petermann, *Laser Diode Modulation and Noise* (Kluwer Academic, Dordrecht, 1988).

[20] N. B. Abraham and D. E. Chyba, Opt. Commun. **85**, 83 (1991).

[21] K. Kikuchi, IEEE J. Quantum Electron. **QE-24**, 1914 (1988).

[22] K. Y. Lau, Appl. Phys. Lett. **52**, 257 (1988).

[23] See, e.g., Ref. [10] (p. 248) and references therein.

[24] G. P. Agrawal, in *Nonlinear Dynamics in Optical Systems*, edited by N. B. Abraham, E. Garmire, and P. Mandel (Optical Society of America, Washington, DC, 1991), p. 28; J. Appl. Phys. **63**, 1232 (1988).

[25] M. Lax, Rev. Mod. Phys. **32**, 25 (1960); in *Laser Noise*, edited by R. Roy, SPIE Proc. No. 1376 (Bellingham, 1991), p. 2; M. Lax and W. H. Louisell, Phys. Rev. **185**, 568 (1969).

[26] D. Marcuse, IEEE J. Quantum Electron. **QE-21**, 154 (1985).

[27] H. Carmichael, *Quantum Statistical Methods in Quantum Optics* (Springer-Verlag, Berlin, in press).

[28] J. H. Eberly, K. Wódkiewicz, and B.W. Shore, Phys. Rev. A **30**, 2381 (1984); **30**, 2390 (1984); G. P. Agrawal, IEEE J. Quantum Electron. **QE-21**, 680 (1985).

[29] W. H. Press, B. P. Flannery, S. A. Teukolsky, and W. T. Vetterling, *Numerical Recipes: The Art of Scientific Computing* (Cambridge University Press, New York, 1986).

[30] G. L. Oppo, J. R. Tredicce, and L. M. Narducci, Opt. Commun. **69**, 393 (1989).

[31] *Handbook of Special Functions*, edited by M. Abramowitz and I. A. Stegun (Dover, New York, 1970).

[32] F. de Pasquale and P. Tombesi, Phys. Lett. A **72**, 7 (1979); F. de Pasquale, P. Tartaglia, and P. Tombesi, Z. Phys. B **43**, 353 (1981); Phys. Rev. A **25**, 466 (1982).